



Human subiculo-fornico-mamillary system in Alzheimer's disease: Tau seeding by the pillar of the fornix

Manon Thierry^{1,2} · Susana Boluda^{1,2} · Benoît Delatour¹ · Serge Marty¹ · Danielle Seilhean² · Brainbank Neuro-CEB Neuropathology Network · Marie-Claude Potier¹ · Charles Duyckaerts^{1,2}

Received: 30 September 2019 / Revised: 29 November 2019 / Accepted: 30 November 2019 / Published online: 10 December 2019
© Springer-Verlag GmbH Germany, part of Springer Nature 2019

Abstract

In Alzheimer's disease (AD), Tau and A β aggregates involve sequentially connected regions, sometimes distantly separated. These alterations were studied in the pillar of the fornix (PoF), an axonal tract, to analyse the role of axons in their propagation. The PoF axons mainly originate from the subicular neurons and project to the mamillary body. Forty-seven post-mortem cases at various Braak stages (Tau) and Thal phases (A β) were analysed by immunohistochemistry. The distribution of the lesions showed that the subiculum was affected before the mamillary body, but neither Tau aggregation nor A β deposition was consistently first. The subiculum and the mamillary body contained Gallyas positive neurofibrillary tangles, immunolabelled by AT8, TG3, PHF1, Alz50 and C3 Tau antibodies. In the PoF, only thin and fragmented threads were observed, exclusively in the cases with neurofibrillary tangles in the subiculum. The threads were made of Gallyas negative, AT8 and TG3 positive Tau. They were intra-axonal and devoid of paired helical filaments at electron microscopy. We tested PoF homogenates containing Tau AT8 positive axons in a Tau P301S biosensor HEK cell line and found a seeding activity. There was no A β immunoreactivity detected in the PoF. We could follow microcryodissected AT8 positive axons entering the mamillary body; contacts between Tau positive endings and A β positive diffuse or focal deposits were observed in CLARITY-cleared mamillary body. In conclusion, we show that non-fibrillary, hyperphosphorylated Tau is transported by the axons of the PoF from the subiculum to the mamillary body and has a seeding activity. Either Tau aggregation or A β accumulation may occur first in this system: this inconstant order is incompatible with a cause-and-effects relationship. However, both pathologies were correlated and intimately associated, indicating an interaction of the two processes, once initiated.

Keywords Alzheimer's disease · Tau · Abeta · Subiculo-fornico-mamillary system · Seeding · Propagation · Biosensor · Microcryodissection · CLARITY · Electron microscopy · Axon propagation

The members of Brainbank Neuro-CEB Neuropathology Network are listed in the Acknowledgements section.

Electronic supplementary material The online version of this article (<https://doi.org/10.1007/s00401-019-02108-7>) contains supplementary material, which is available to authorized users.

✉ Charles Duyckaerts
charles.duyckaerts@aphp.fr

¹ Alzheimer's and Prion Diseases Team, Paris Brain Institute, CNRS, UMR 7225, INSERM 1127, Sorbonne University UM75, Paris, France

² Laboratoire de Neuropathologie Raymond Escourolle, Pitié-Salpêtrière Hospital, APHP, Sorbonne University, 47, Blvd de l'Hôpital, 75651 Paris Cedex 13, France

Introduction

Alzheimer's disease (AD) is characterised by extracellular accumulation of β -amyloid peptides (A β) and intracellular aggregation of hyperphosphorylated Tau proteins (hp-Tau). A β peptides accumulate in different types of extracellular deposits (diffuse, focal, neuritic, stellate and subpial [13]), while hp-Tau aggregates in the neuronal soma, leading to the formation of neurofibrillary tangles (NFTs) [7, 30]. Accumulation of hp-Tau in neurites leads to the formation of neuropil threads, thought to be mainly dendritic [5], while the hp-Tau positive neurites of the corona of the senile plaques are thought to be mainly axonal [53]. Thal phases (from 0 to 5) evaluate the progression of A β deposits [59] and Braak neurofibrillary stages (from 0 to VI), of hp-Tau accumulation [2].

Misfolded Tau proteins injected in Tau transgenic mice, which are too young to develop lesions induce early development of Tau aggregates that apparently propagate like a prion, following neural circuits [10]. A β pathology is also able to propagate in a prion-like way [47]—hence the term propagon that has been suggested for these protein assemblies [20]. The mechanism and kinetics of the initiation and propagation of Tau and A β lesions are still poorly understood, both in experimental animals and in humans. The amyloid cascade hypothesis [33, 54] posits that A β peptide aggregation is an early pathological process driving Tau phosphorylation, neurofibrillary tangle formation, synaptic loss and neuronal death.

We studied the subiculo-fornico-mamillary system in the human brain, to analyse the progression of Tau and A β pathologies, their timing and their relationship. The fornix, localised below the corpus callosum, is laterally limited on each side by the pillar of the fornix (PoF), a large intra-hemispheric associative bundle, 4.5 cm long and 0.75 cm in diameter. That bundle, a key element of the Papez circuit, links the hippocampal formation (including the subiculum) with the mamillary body, the septal and the accumbens nuclei [62] (Fig. 1a). The PoF is exclusively made of axons that can thus be studied in isolation, while they are difficult to identify in the neuropil, where they are mixed with dendrites. The PoF degenerates during AD [11]. The abundance of fibres of hippocampal origin in the PoF is illustrated by fornico-mamillary atrophy, in which neuronal loss in the hippocampus causes atrophy of the PoF and of the mamillary body (Fig. 1b). The majority of the axons travelling in the PoF originate from the neurons of the subiculum, where NFTs form as early as Braak stage III and amyloid

deposits are seen at Thal phase 2. Those axons project to the mamillary body, where NFTs appear from Braak stage IV and A β peptides accumulate at Thal phase 3 [2, 59]. The hippocampo-fornico-mamillary system is vascularised by different arteries: the posterior cerebral artery for the subiculum, the anterior communicating artery for the mamillary body [34]; diffusion through the vascular system is thus implausible. As both structures are wide apart, passive diffusion from one to the other is also unlikely. This system is thus well suited to investigate the propagation of Tau and A β lesions through defined axonal connections.

Materials and methods

Cases

Forty-seven post-mortem brains were investigated. All the brains had been removed and collected at Pitié-Salpêtrière hospital (Paris). They were stored in 4% formalin. In all the cases, the diagnostic procedure included A β (6F3D, Dako), Tau (AT8, Thermo-Fisher), α -synuclein (5G4, Sigma-Aldrich) and TDP-43 (Proteintech Group) immunohistochemistry. The hippocampus, the PoF and the mamillary body were analysed for each case. Among the 47 cases that we studied, 38 brains had been collected in a brain donation project and stored in the French national brain biobank Neuro-CEB (Bioresource Research Impact Factor number = BRIF BB-0033-00011). The cohort was composed of 15 women and 32 men, aged 51–96 (Table 1). The cases included 28 patients with no or asymptomatic AD lesions, deceased of other causes (Braak 0–IV) and 19 patients with

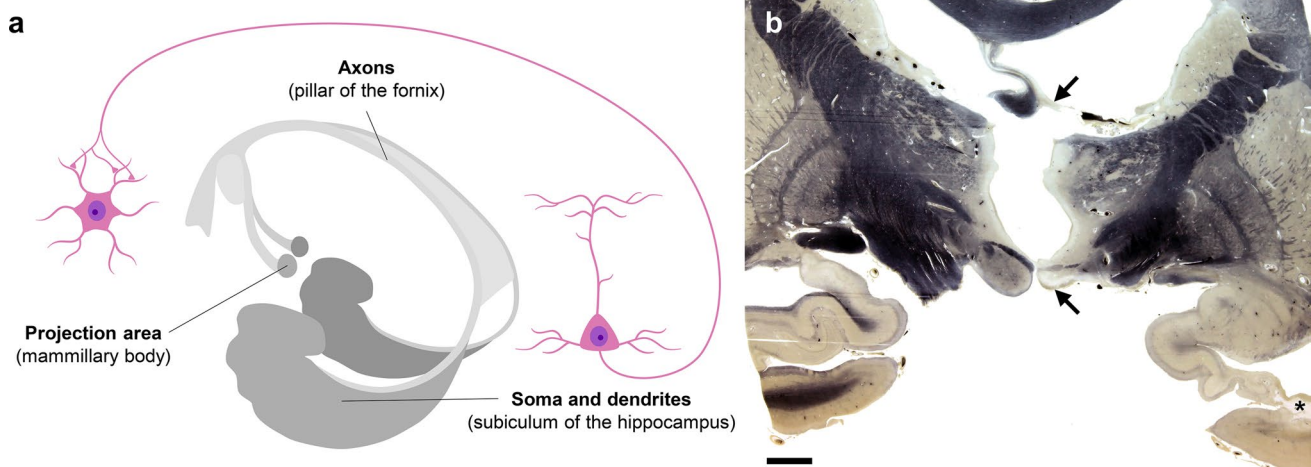


Fig. 1 The subiculo-fornico-mamillary system. **a** Anatomy of the subiculo-fornico-mamillary circuit. **b** Unilateral atrophy of the pillar of the fornix (upper arrow) and of the ipsilateral mamillary body (lower arrow) caused by an infarct of the subiculum (asterisk) in the

right hippocampus, demonstrating the importance of the subiculo-mamillary connections through the pillar of the fornix. Illustrative case from Escourolle Neuropathology Collection. Brain coronal section. Loyez myelin stain. Scale bar 5 mm

Table 1 Cases

Case	Braak (Tau)	Thal	Braak (α -synuclein)	Age	Gender	Diagnosis
Neuropathological analysis ($n = 47$)						
01	0	0	0	51	M	Coronary atheroma and fungal pneumopathy
02	0	1	0	66	M	Acute myeloblastic leukaemia
03	I	0	0	65	M	Brain donation. Some ischemic neurons
04	I	1	0	74	F	Ischemic lesions
05	II	3	0	83	M	Large T-cell lymphoma
06	II	0	0	62	M	Ischemic cardiopathy, infarcts in contralateral hemisphere
07	II	1	0	81	M	Brain donation. Control
08	II	1	5	67	M	Parkinson's disease. Cortical Lewy bodies
09	III	2	0	85	M	Perirenal angiosarcoma with pulmonary metastases
10	III	4	0	73	F	Peritonitis and acute bronchopneumopathy
11	III	0	0	75	M	Cardio-respiratory arrest after parotidectomy. Some dilations of the perivascular space in the basal ganglia
12	III	4	5	84	M	Diffuse Lewy-body disease. High probability ^a
13	III	0	0	71	M	Peritonitis
14	III	0	0	54	F	Cirrhosis, and pulmonary infarction
15	III	0	0	92	F	Brain donation. Control
16	III	0	5	60	F	Parkinson's disease. Cortical Lewy bodies
17	III	3	6	84	M	Diffuse Lewy-body disease. High probability ^a
18	III	0	0	66	M	Cirrhosis
19	III	0	0	70	F	Brain donation. Minimal neuropathological changes. Type 2 CAA (meninges)
20	III	0	0	53	M	Sudden death
21	IV	2	0	86	M	Brain donation. Myocardial infarct. Type 1 CAA
22	IV	3	0	85	F	Lacune of the pons. Sclerohyalinosis
23	IV	3	0	71	M	Acute pancreatitis and cirrhosis
24	IV	4	0	74	M	Metastatic adenocarcinoma
25	IV	1	6	85	M	Parkinson's disease. Cortical Lewy bodies
26	IV	3	6	81	M	Parkinson's disease. Cortical Lewy bodies, argyrophilic grain disease, lacune of the pallidum, old occipital infarct
27	IV	3	6	84	M	Diffuse Lewy-body disease, High probability ^a . CAA (type 2)
28	IV	0	0	90	F	Non-demented individual with tau AD-related lesions
29	V	4	0	76	M	AD
30	V	5	6	81	M	AD, diffuse Lewy-body disease. Low probability ^a
31	V	4	6	76	F	AD, diffuse Lewy-body disease. Intermediate probability ^a
32	V	5	0	92	M	AD, Ammon's horn sclerosis and TDP-43 inclusions
33	V	4	6	87	M	AD, diffuse Lewy-body disease. Intermediate probability ^a
34	V	4	0	81	F	AD
35	V	4	Amygdala only	96	F	AD, amygdala Lewy bodies
36	V	5	6	80	M	AD, diffuse Lewy-body disease. Intermediate probability ^a
37	V	5	6	74	F	AD, diffuse Lewy-body disease. Intermediate probability ^a
38	VI	5	0	78	F	AD
39	VI	3	0	86	M	AD
40	VI	2	0	79	M	AD
41	VI	5	Amygdala only	73	F	AD, amygdala Lewy bodies
42	VI	5	0	68	F	Posterior cortical atrophy. AD
43	VI	5	0	79	M	AD
44	VI	5	0	60	M	AD
45	VI	5	0	66	M	AD
46	VI	4	0	79	M	AD
47	VI	3	0	65	M	AD

Table 1 (continued)

Case	Braak (Tau)	Thal	Braak (α -synuclein)	Age	Gender	Diagnosis	Technique(s)
Additional analyses ($n=6$)							
48	0	0	0	62	F	Multi-organ dysfunction syndrome	Electron microscopy
49	0	0	0	39	M	Brainstem glioma (samples were taken from uninvolved pillars of the fornix)	Cell culture
50	IV	5	0	91	M	AD	Cell culture, electron microscopy
51	VI	5	Amygdala only	61	F	AD, amygdala Lewy bodies	Microcryodissection
52	VI	5	0	81	F	AD	Clarity, electron microscopy
53	VI	5	0	76	M	AD	Cell culture

The cases are sorted according to Braak neurofibrillary stages [2]. “Braak (Tau)” stands for Braak and Braak neurofibrillary stages [2]; “Thal” refers to Thal et al. phases [59] and “Braak (α -synuclein)” indicates Braak et al. staging of synucleinopathy, related to sporadic Parkinson’s disease [6]. The hippocampus and the pillar of the fornix were sampled in all 47 cases. The hippocampus was studied in slices cut perpendicularly to its long axis. The fornix was cut parallel to its main axis. The mamillary body was studied in 41 cases (in 6 cases, the mamillary body was not available or too altered to be analysed). Six additional cases were sampled for microcryodissection and CLARITY techniques (two formalin-fixed mamillary bodies), electron microscopy analysis (three formalin-fixed transversal sections of hippocampus and three formalin-fixed longitudinal sections of the pillar of the fornix) and cell culture (three frozen pillars of the fornix)

AD Alzheimer’s disease, CAA cerebral amyloid angiopathy, PD Parkinson’s disease

^aThe probability refers to the “assessment of the likelihood that the pathologic findings are associated with a typical, dementia with Lewy bodies, clinical syndrome”, from McKeith et al. [46]

established AD (Braak V–VI). Among the 28 asymptomatic patients, 17 had mild Tau alterations associated with no or only little A β accumulation (Thal phase 1 or 2). It is common to observe cases with Tau pathology in the entorhinal area and hippocampus and no A β accumulation in the brain ([3], see also the prevalence curves obtained from the data of [3] in the companion paper [15]). Those cases have been recently isolated under the name of PART [12], a questionable construct [18]. Fourteen cases had Lewy bodies. Cases diagnosed with primary tauopathies were excluded from the study (i.e. progressive supranuclear palsy, corticobasal degeneration, *MAPT* mutation, argyrophilic grain disease, Pick’s disease). The eight cases at Braak 0/I/II corresponded to control brains with no lesion in the hippocampus. Some Tau pathology was present in the subiculum in the 20 cases at Braak III/IV. The 19 cases at Braak V/VI had extensive Tau pathology in the subiculum, but also in the neocortex. Thal phases ranged from 0 to 5 (Table 1). Six additional cases (also listed in Table 1) were used for CLARITY, microcryodissection, electron microscopy analysis and cell culture seeding assays. The project was submitted to the “committee for the protection of persons” (ethical committee) Ile de France VI which did not object the study (April 20th 2016 session).

Histology analysis

The hippocampus, PoF and mamillary body were sampled after a fixation of at least 2 months in a 10% formalin solution (containing 4% formaldehyde). The samples were embedded in paraffin. The PoF was dissected and embedded

parallel to its long axis over a distance of at least 1 cm. The blocks were cut at a thickness of 3 μ m.

Immunohistochemistry

Immunohistochemistry was performed with the Nexes station automated system (Ventana Medical System Inc., Roche). Deparaffinised and rehydrated sections were pre-treated and blocked, then incubated with the primary antibodies listed in Supplementary Table 1, online resource. The AT8, TG3, PHF1, Alz50, C3 and anti-myelin basic proteins (MBP) primary antibodies were detected with the *ultraView* Universal DAB Detection kit (Ventana Medical System Inc., Roche) or *OptiView* DAB immunohistochemistry Detection kit (Ventana Medical System Inc., Roche), according to the automated procedure summarised in supplementary Table 1, online resource. The kits include secondary antibodies (goat anti-mouse IgG, anti-mouse IgM and anti-rabbit) conjugated with horseradish peroxidase (HRP). The addition of H₂O₂ and diaminobenzidine leads to the formation of a brown precipitate in presence of HRP. The anti-A β 6F3D immunohistochemistry was performed manually following formic acid pretreatment (98% formic acid for 5 min); the primary antibody was incubated overnight. The MBP/Neurofilament and A β /Tau double immunostaining made use of the same protocol as previously described for the first primary antibody (anti-MBP and anti-A β 6F3D, respectively). The second primary antibody (anti-Neurofilament and AT8 anti-Tau, respectively) was revealed with the *ultraView* Universal Alkaline Phosphatase Red Detection kit (Ventana Medical System Inc., Roche), according to the automated procedure summarised in supplementary Table 1, online resource. The

detection kit includes secondary antibodies (goat anti-mouse IgG, anti-mouse IgM and anti-rabbit) conjugated with alkaline phosphatase (AP) and reagents (naphtol and fast red), leading to the formation of a red precipitate in presence of AP. The slides were counterstained with Harris haematoxylin and dehydrated. Coverslips were mounted in Pertex (Histolab, Labelians).

Gallyas silver impregnation

Gallyas method [27] was applied with the modifications proposed by Uchihara et al. [61] that result in the bleaching of the undesired myelin staining. The slides were counterstained with 0.1% nuclear fast red and dehydrated. Coverslips were mounted in Pertex (Histolab, Labelians).

Quantifications

An area covering the whole thickness of the subiculum was systematically observed with a 20× objective after AT8, TG3, Alz50, PHF1, and C3 anti-Tau immunohistochemistry and Gallyas staining. One hundred neuronal profiles and ghost tangles were examined. The proportion of neuronal profiles (total number of neurons as denominator) with pre-tangles, NFTs and ghost NFTs was assessed. A pilot study [31] had determined that the error coefficient improved only slowly when the number of assessed profiles was above 100. The percentages of positive profiles were converted into grades from 0 to 3 (0: 1% or less; 1: from 2 to 34%; 2: from 35 to 67%; 3: 68% or more). The volume density of A β deposits in the subiculum was estimated by point counting after anti-A β 6F3D immunohistochemistry [66]. A video camera transmitted the picture of the subiculum to a screen on which a grid of points was superimposed. The points were regularly spaced at 80 μ m intervals (9 rows \times 12 columns). The proportion of points falling onto A β immunoreactive material over a total of 100 points (\pm 10, depending on the size of the subiculum) was counted to estimate the areal density A_A [number of points falling onto A β immunoreactive material]/[total number of points]. A_A is an unbiased estimator of the volume ratio V_V [volume of A β deposits]/[total volume], according to Delesse principle ($A_A = V_V$) [66]. As A β was heterogeneously distributed, we chose to evaluate the areas in which the density appeared to be the highest: the assessment thus concerned the highest (rather than the mean) proportion of volume. The numerical densities of AT8, TG3, Alz50, PHF1, C3 and Gallyas positive axons were semi-quantitatively assessed on longitudinal sections of the PoF after adequate immunohistochemistry or staining. The following scale was applied: 0: no staining (1% of the labelled axons or less); 1: rare and patchy staining (from 2 to 34%); 2: staining with intermediate density (from 35 to 67%); 3: staining with high density (68% or more). In

the mamillary body, the density of AT8, TG3, Alz50, PHF1, C3 and Gallyas positive pre-tangles, NFTs and ghost NFTs was semi-quantitatively assessed as previously (from grade 0 to 3) as well as the volume proportion of A β deposits.

Density maps of the lesions in the mamillary body

Voronoi (or “Dirichlet”) tessellation was used to draw quantitative maps of the numerical density of the lesions in the mamillary body [16]. The maps were drawn with an apparatus made of a video system, of linear transducers fastened to the moving stage of the microscope, and of a computer with a mouse. The microscopic picture was visible on the computer screen. The mouse allowed drawing the contour of the studied region and pointing the Tau AT8 positive NFT or pre-tangles and the A β 6F3D positive deposits. The borders of the medial and lateral nuclei of the mamillary body were manually drawn on the video screen with the mouse. The transducers associated the points that had been drawn with X and Y coordinates [29] and guaranteed that they followed the movement of the microscope stage. Maps of A β deposits and AT8 Tau positive neuronal profiles were obtained. Coordinates of the borders of the medial and lateral nuclei of the mamillary body, and of the pointed lesions were stored in a file at the end of the acquisition step. These coordinates were used to analyse the data with a specially devised tessellation program. The region was divided into polygons limited by sides located at mid-distance of two neighbouring lesions and perpendicular to the line that joined them. Each polygon contained only one labelled lesion (A β deposit or neurofibrillary tangle or pretangle). The polygons covered the entire area of the region without overlaps or interstices, i.e. “tessellated” the plane. The area of each individual polygon is inversely proportional to the numerical density of the pointed lesions that it contains. When the density is high, the lesions are close to each other and the polygons are small. Assigning a colour to a range of polygon areas allowed drawing a ‘heatmap’ of the numerical density of the lesions [14, 16].

In vitro seeding experiments

Preparation of PoF homogenates

Approximately 100 mg of frozen PoF sampled from cases 49, 50 and 53, listed in Table 1, were thawed on ice. The tissue was mixed with ice-cold phosphate-buffered saline (PBS) containing protease and phosphatase inhibitor cocktail (Thermo Scientific) to obtain a final solution of 10% weight/volume. Tissue was homogenised by 15–20 strokes in a 1 mL glass homogeniser (Fisher Scientific), briefly sonicated on ice with a Misonix Q125 sonicator (Q-sonica) and clarified by centrifugation (3000g, 5 min, 4 °C) as previously

described [10]. Supernatants were collected, aliquoted and stored at -80°C .

Preparation and treatment of biosensor cells sensitive to Tau seeding

Tau P301S biosensor HEK cells (#CRL-3275, ATCC, LGC Standards [38]) were grown in complete culture medium (DMEM with 10% FBS and 1% penicillin/streptavidin, Gibco, Thermo Fisher Scientific). They were treated with clarified PoF homogenates as in [26, 38] with minor modifications. Approximately 170,000 cells contained in 650 μL of complete medium were plated, per well, in a 24-well plate and left overnight in the incubator (37°C , 5% CO_2 and $\geq 80\%$ relative humidity). At around 60% of confluence, 100 μL of a transduction mix containing the PoF homogenate was added per well, in duplicate. The transduction mix was obtained by combining 43.75 μL Opti-MEM (Gibco, Thermo Fisher Scientific) and 6.25 μL Lipofectamine 2000 (Invitrogen, Thermo Fisher Scientific), with 12.5 μL of PoF homogenate added to 37.5 μL Opti-MEM. The transduction mix was briefly spun, then incubated for 1 h at room temperature, before being added to the cells. Treated cells were left in the incubator during 48 h. The experiment was replicated thrice.

Analysis

After treatment, cells were rinsed with PBS and re-plated on 13 mm diameter coverslips coated with poly-D-lysine (Sigma-Aldrich). The coverslips were left overnight in the incubator. They were rinsed with PBS and fixed for 10 min in 4% PFA. The cells were counterstained for 10 min with DAPI in 0.05% Triton X-100. The coverslips were mounted with Fluoromount (Sigma-Aldrich). Slides were stored in the dark at 4°C until observation with an inverted confocal Leica TCS SP8 DLS (Leica Microsystems). The CFP-positive cells were manually counted on the confocal images.

A β immunoassay

A β immunoassay of the clarified PoF homogenates, prepared as described above, was performed with the V-PLEX Plus A β Peptide Panel 1 (6E10) kit (Meso Scale Discovery), following the instructions of the manufacturer. A clarified frontal cortex homogenate derived from an AD brain (Braak VI, Thal 5) was used as positive control.

Electron microscopy

The aim was to observe, with electron microscopy, AT8 positive axonal threads present in the PoF. The subiculum and the PoF were sampled from two AD formalin-fixed

brains (cases 50 and 52). An additional PoF was sampled from a formalin-fixed brain devoid of any AD lesions and was used as control (case 48). The samples were sliced into 200 μm thick sections using a vibratome VT 1000S (Leica Microsystems). The PoF was cut along its longitudinal axis and the subiculum perpendicular to its long axis. No AT8 Tau labelling was observed with the immunogold method that appeared unsuitable for post-mortem formalin-fixed material. We thus used the direct visualisation of diaminobenzidine precipitates after AT8 Tau immunohistochemistry was performed without pretreatment and without detergent on the vibratome slices. Regions of interest (with an area of 1 mm^2) were dissected on the slices. The samples were washed in phosphate buffer and transferred into a 1% osmium solution for 1 h. After several washes in water, they were stained “en bloc” with a 5% uranyl acetate solution for 30 min. The samples were dehydrated in graded ethanol (from 50 to 100%) followed by acetone. They were incubated in 50% acetone—50% epon overnight, followed by pure epon for 2 h, before being cured at 60°C for 48 h in a dry oven. Semi-thin (0.5 μm) and ultrathin (70 nm) sections were cut using an EM UC7 (Leica Microsystems). Ultrathin sections were collected on copper grids and analysed with a Hitachi HT700 electron microscope (Hitachi, Milexia) operating at 100 kV. Pictures were taken with 2048×2048 AMT R41-B CCD camera (AMT, Milexia).

Microcryodissection

One formalin-fixed mamillary body was sampled from an additional AD case (case 51). The sample was microcryodissected following the procedure previously described [60]. Briefly, cycles of freezing and thawing induce changes in the water volume contained in the sample, ice occupying more space than water. Repeated cycles separate the elements of the tissue. The sample was rinsed and left in water on a Peltier module. Three-hundred and twenty freezing and thawing cycles were achieved (program settings: 700 s ‘on’, freezing; 300 s ‘off’, thawing). Microcryodissected mamillary body was embedded in paraffin and analysed by immunohistochemistry as described above.

CLARITY

A 3 mm thick slice of a formalin-fixed mamillary body was taken from an AD case (< 1 year fixation; Braak VI, Thal 5; Case 52) and processed by the CLARITY technique adapted to post-mortem tissue [1]. The sample was embedded in an acrylamide hydrogel constituted of 4% acrylamide and 0.25% temperature-triggering initiator VA-044 in PBS. The sample was thoroughly washed in the clearing solution (200 mM boric acid, 4% SDS, pH 8.5) and placed in the X-CLARITY tissue clearing system (Logos Biosystems

Inc.). A direct current (1.5 A) and a constant flow of clearing solution heated to 40 °C were applied during a total of 96 h. The clearing solution was renewed every 24 h. After clearing, the sample was pretreated with formic acid 98% for 15 min. The tissue was blocked with 10% of goat and donkey sera (with a 1:1 ratio). The sample was incubated with a mouse monoclonal antibody anti-A β (4G8, BioLegend) and a rabbit polyclonal antibody anti-total-Tau (B19, gift from J.-P. Brion, Free University of Brussels, Belgium). Donkey anti-mouse Alexa 488 and goat anti-rabbit Alexa 555 (Life Technologies, Thermo Fisher Scientific) were used as secondary antibodies. The sample was post-fixed in 4% paraformaldehyde and autofluorescence was quenched with 0.2 M glycine. The day before observation, the tissue was mounted with RapidClear[®]. The microscope analyses were made with an upright multiphoton Zeiss 710 NLO (Carl Zeiss Microscopy). The images were post analysed with Fiji (Fiji Is Just ImageJ, National Institutes of Health) and Imaris (Bitplane, Oxford Instruments).

Statistical analyses

All the data were analysed with GraphPad Prism 6, at a significance level of 5%. For discrete neuropathological data, non-parametric statistical tests were performed: Spearman test was used for analysis of correlation, Kruskal–Wallis and Friedman tests were used for one-way analysis of variance (respectively for untied or tied data) followed by Dunn's post hoc multiple comparisons when the null hypothesis was rejected. The means of groups with or without Lewy bodies were compared with Mann–Whitney. To illustrate the relationship between the data, we also drew a regression line with the hp-Tau semi-quantitative measures (Supplementary Figs. 2 and 3, online resource), with the hypothesis that the discrete data describing a severity gradient could be interpolated by the regression between the grades and that the grades had a binomial tending to a Gaussian distribution. In the seeding experiments, the number of CFP-positive HEK cells was expressed as a percentage of the total cell number counted. The mean percentages were compared using a Student *t* test, performed after an arcsine square root transformation (as recommended, [56] to approach a normal distribution).

Results

Distribution of Tau and A β accumulation in the subiculo-fornico-mamillary system

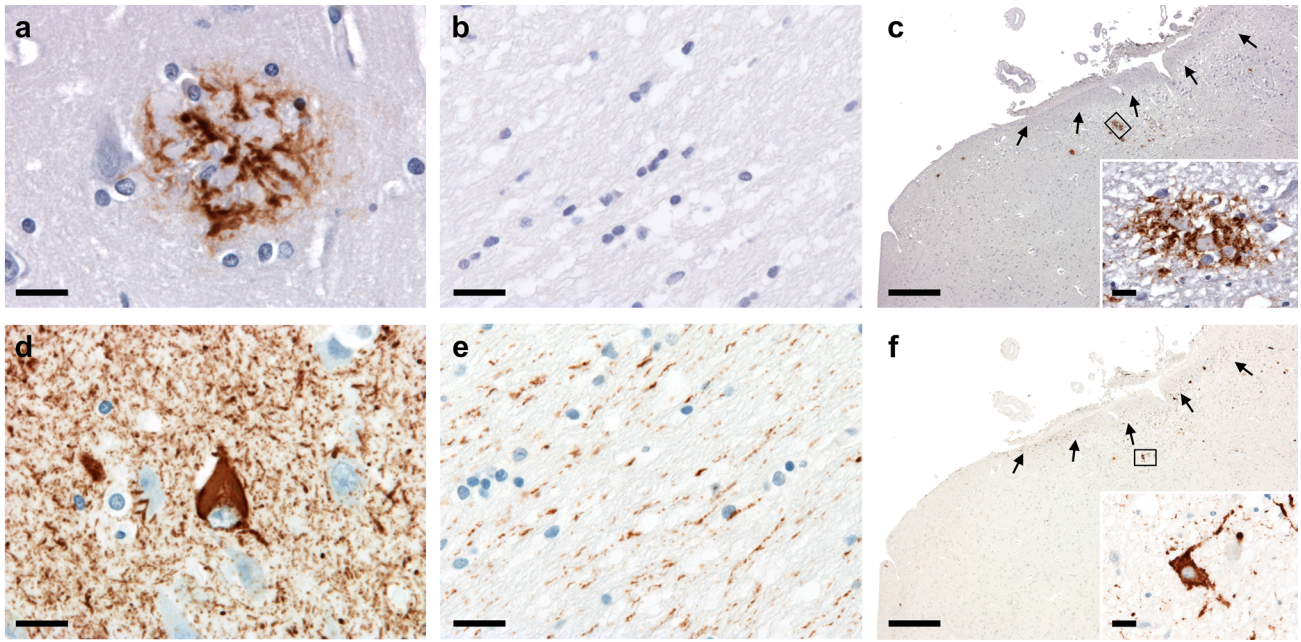
A β deposition in the subiculo-fornico-mamillary system

A β deposits were observed in the subiculum and in the mamillary body (Fig. 2a, c). No A β immunoreactivity was

detected in or around the axons of the PoF (Fig. 2b). This result was confirmed by A β 40 and A β 42 immunoassays in PoF homogenates from three cases at Braak stages 0 (negative control), IV and VI. In the PoF homogenates, A β 40 and A β 42 concentrations were below 2% and 8.5% of the positive control values, respectively. The volume proportions of A β deposits in the subiculum and in the mamillary body were positively correlated (Spearman test, $\rho_S = 0.720$, $p < 0.0001$). A β deposits were observed in the subiculum in 27 cases, in the absence of deposit in the mamillary body in two cases, while A β deposits in the mamillary body (25 cases) were systematically associated with A β deposits in the subiculum (Fig. 2g, i; supplementary Fig. 1, online resource). Lewy pathology did not modify A β accumulation (Mann–Whitney test, $p > 0.05$).

Hp-Tau accumulation in the subiculo-fornico-mamillary system

Pre-tangles, neurofibrillary and ghost tangles were observed in the subiculum and mamillary body (Fig. 2d, f). Only axonal threads, made of thin and fragmented AT8 positive axons, were found in the PoF (Fig. 2e). Three groups of cases (control, intermediate, severe) were then considered according to Braak neurofibrillary stages (Fig. 2j). In the eight control cases (Braak 0, I, II), no Tau AT8 immunoreactivity was, by definition, observed in the subiculum; Tau positive accumulation was also absent in the PoF and in the mamillary body. In the 20 intermediate cases (Braak III, IV), hp-Tau accumulations were detected in the subiculum and PoF, but were scarce in the mamillary body. In the 19 severe cases (Braak V, VI), they were abundant in the subiculum, PoF and to a lesser extent, in the mamillary body. Hp-Tau accumulation in the PoF was correlated both with hp-Tau accumulation in the subiculum, its area of origin (Spearman test, $\rho_S = 0.885$, $p < 0.0001$) and in the mamillary body, its target area (Spearman test, $\rho_S = 0.724$, $p < 0.0001$). The cases with hp-Tau accumulation in the subiculum, PoF, and mamillary body could be hierarchically ranked. Tangles in the subiculum were associated with axonal threads in the PoF in all but one case. Axonal threads in the PoF were systematically associated with tangles in the subiculum. Similarly, axonal threads in the PoF were observed in the absence of tangles in the mamillary body, while tangles in the mamillary body were always associated with axonal threads in the PoF (Fig. 2h; supplementary Fig. 2, online resource). Lewy pathology had no influence on the abundance and topography of hp-Tau accumulation (Mann–Whitney test, $p > 0.05$).



g

Cases	Sub-Aβ	PoF-Aβ	MB-Aβ
01	-	-	-
02	-	-	-
04	-	-	-
06	-	-	-
07	-	-	-
11	-	-	-
13	-	-	-
16	-	-	-
18	-	-	-
19	-	-	-
20	-	-	-
21	-	-	-
24	-	-	-
28	-	-	-
10	+	-	-
14	+	-	-
05	+	-	+
09	+	-	+
17	+	-	+
22	+	-	+
23	+	-	+
25	+	-	+
26	+	-	+
29	+	-	+
30	+	-	+
31	+	-	+
32	+	-	+
33	+	-	+
34	+	-	+
36	+	-	+
37	+	-	+
38	+	-	+
39	+	-	+
40	+	-	+
41	+	-	+
42	+	-	+
43	+	-	+
44	+	-	+
45	+	-	+
46	+	-	+
47	+	-	+
03	-	-	NA
08	-	-	NA
15	-	-	NA
12	+	-	NA
27	+	-	NA
35	+	-	NA

h

Cases	Sub-Tau	PoF-Tau	MB-Tau
01	-	-	-
02	-	-	-
04	-	-	-
05	-	-	-
06	-	-	-
07	-	-	-
24	+	-	-
09	+	+	-
11	+	+	-
13	+	+	-
14	+	+	-
16	+	+	-
19	+	+	-
20	+	+	-
21	+	+	-
23	+	+	-
29	+	+	-
37	+	+	-
10	+	+	+
17	+	+	+
18	+	+	+
22	+	+	+
25	+	+	+
26	+	+	+
28	+	+	+
30	+	+	+
31	+	+	+
32	+	+	+
33	+	+	+
34	+	+	+
36	+	+	+
38	+	+	+
39	+	+	+
40	+	+	+
41	+	+	+
42	+	+	+
43	+	+	+
44	+	+	+
45	+	+	+
46	+	+	+
47	+	+	+
03	-	-	NA
08	-	-	NA
12	+	+	NA
15	+	+	NA
27	+	+	NA
35	+	+	NA

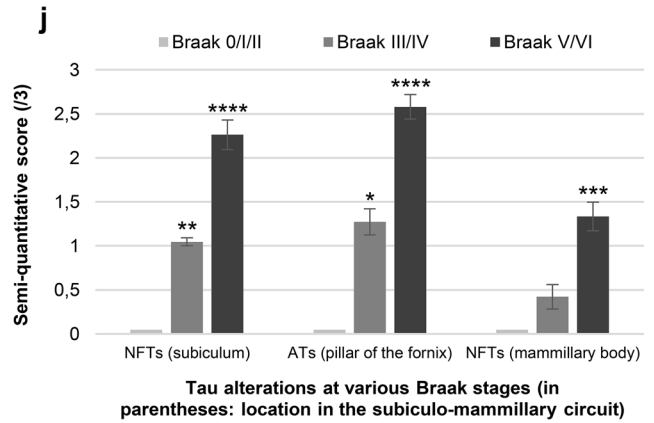
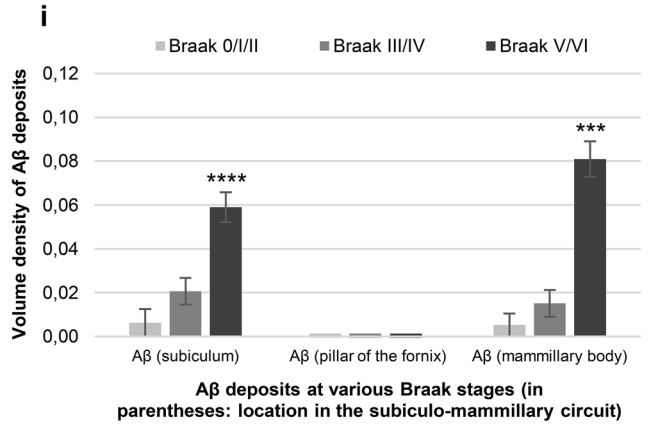


Fig. 2 Accumulation of hyperphosphorylated Tau and A β in the subiculo-fornico-mamillary system; A β deposits are found in the subiculum and mamillary body, but not in the pillar of the fornix. All the pictures have been taken from case 30. **a** A β deposits in the subiculum, anti-A β 6F3D immunohistochemistry (scale bar 20 μ m). **b** No accumulation of A β was detected in the pillar of the fornix after anti-A β 6F3D immunohistochemistry (scale bar 20 μ m). **c** A β deposits in the mamillary bodies, anti-A β 6F3D immunohistochemistry (scale bar 400 μ m). Insert: higher magnification of the rectangle showing the deposits (scale bar 20 μ m). **d** Tangles in the subiculum, anti-hp-Tau AT8 immunohistochemistry (scale bar 20 μ m). **e** Axonal threads made of thin and fragmented hp-Tau AT8 positive axons, in the pillar of the fornix (scale bar 20 μ m). **f** Tau pathology (pre-tangles, tangles and threads) in the mamillary body after AT8 anti-hp-Tau immunohistochemistry. Many axonal threads from the pillar of the fornix were seen at the periphery of the mamillary body, at the ending of the PoF (scale bar 400 μ m). Insert: higher magnification of the rectangle showing an AT8 positive neuron (scale bar 20 μ m). **g** Absence (–, light grey) or presence (+, dark grey) of A β deposits in the subiculum (Sub), pillar of the fornix (PoF) and mamillary body (MB). NA not available: six mamillary bodies could not be sampled; the six corresponding cases were excluded from the analysis of the hierarchical distribution (in grey, end of the table). **h** Absence (–, light grey) or presence (+, dark grey) of hp-Tau AT8 positive pre-NFTs, NFTs and ghost NFTs in the subiculum and mamillary body, and of hp-Tau AT8 positive threads in the pillar of the fornix. **i** Mean volume density of A β deposits as a function of Braak stages (Kruskal–Wallis and Dunn’s post tests in comparison with the control group, which included cases at Braak stages 0/II/III, *** p < 0.001, **** p < 0.0001). Error bars: Standard error of the mean. **j** Mean numerical density (semi-quantitative score) of hp-Tau AT8 positive changes as a function of Braak stage, in the subiculum, pillar of the fornix and mamillary body (Kruskal–Wallis and Dunn post-test in comparison with the control group which included cases at Braak stages 0/II/III: * p < 0.05, ** p < 0.01, *** p < 0.001, **** p < 0.0001). NFTs neurofibrillary tangles, ATs axonal threads. Error bars: standard error of the mean

Topography of A β deposits and hp-Tau accumulation in the mamillary body

A β was distributed peripherally, centrally or both peripherally and centrally in the mamillary body. The peripherally located deposits occupied a circular zone at the border of the medial nucleus of the mamillary body; they were stellate or irregular and diffuse. The central deposits were spherical, diffuse or focal (Fig. 3a, c, e). Most of the peripheral distributions were observed in the least affected cases (five cases at Braak < V and Thal < 4 for a total of six peripheral distributions). The central, or central and peripheral distributions were observed in the most advanced cases (14 cases among 19 with those distributions).

The topography of intraneuronal hp-Tau aggregation in the medial nucleus of the mamillary body started and predominated laterally close to the arrival of the PoF. The severity of the involvement of the lateral nucleus was in striking contrast with the relatively moderate changes observed in the medial nucleus (Fig. 3b, d, f). To illustrate the heterogeneity of distribution of A β accumulation and hp-Tau positive

pre-NFTs and NFTs, we drew density maps in six cases at various degrees of severity (Fig. 4).

Seeding properties of axonal Tau species in the PoF

The distribution of Tau pathology in the subiculo-fornico-mamillary system suggested an axonal progression of the pathology from the subiculum to the mamillary bodies through the PoF. To ascertain that possibility, we determined whether the AT8 positive accumulation observed in the PoF had seeding properties in Tau P301S biosensor HEK cells, co-expressing Tau P301S-CFP (cyan fluorescent protein) and Tau P301S-YFP (yellow fluorescent protein). PoF homogenates, containing AT8 positive axons (i.e. enriched in hp-Tau), indeed induced the development of numerous CFP positive inclusions of Tau P301S in the biosensor cells (Fig. 5b–d), contrarily to the homogenate obtained from a control PoF, devoid of any hp-Tau AT8 positive accumulations (Fig. 5a, d). CFP and YFP signals were colocalised.

Characterisation of PoF Tau molecular species, associated with a seeding activity

Phosphorylation and conformation features of Tau axonal threads in the PoF

To identify the molecular Tau species associated with the PoF seeding properties, TG3, PHF1, Alz50, C3 Tau immunohistochemistry and Gallyas silver impregnation were performed in a subset of 19 cases comprising four control cases (Braak 0, I, II), eight intermediate AD cases (Braak III, IV) and seven advanced AD cases at Braak VI (Fig. 6a–d). Tau axonal pathology observed in intermediate cases (Braak III, IV) was associated only with AT8, TG3 and to a lesser extent PHF1 positive axonal threads. A few Alz50 and C3 positive dots were additionally observed in the severe cases (respectively, six and five cases among seven severe cases). Only two severe cases had a few Gallyas positive threads (Fig. 7). Since the seeding activity was detected even in the case of intermediate severity, in which axons of the PoF were found to be only AT8, TG3, and PHF1 positive, we concluded that the seeding activity could still be present in the absence of misfolded, fibrillary or truncated Tau (Alz50, Gallyas and C3 negative).

Electron microscopy analysis of axonal Tau accumulations

Paired helical filaments (PHFs) were frequently observed in the subiculum at electron microscopy, but not within the axons of the PoF derived from the same AD case (Fig. 8a, b). Tau accumulation in the PoF was located in the axoplasm and did not involve the myelin sheath. DAB electron-dense precipitates did not permit identifying

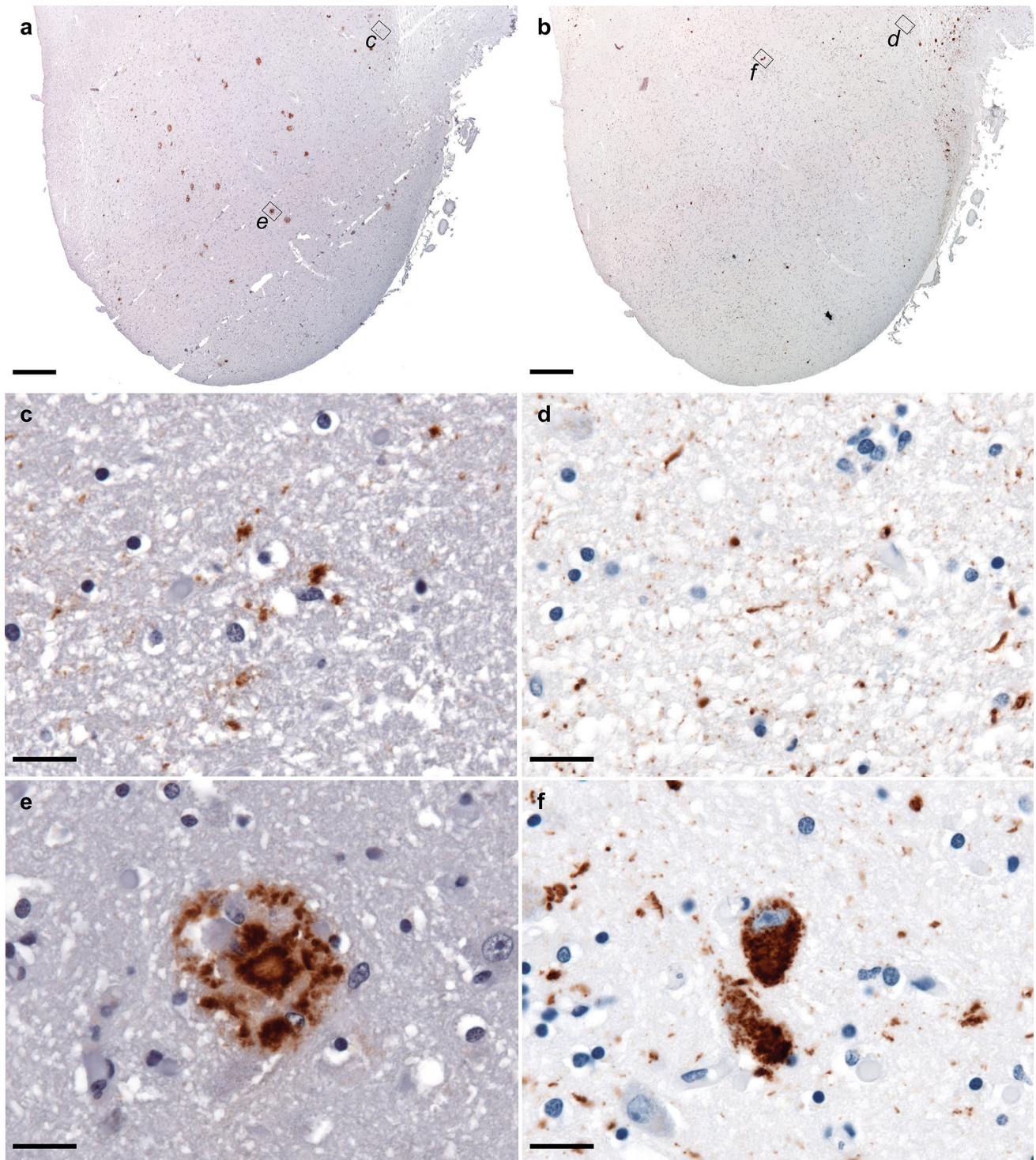


Fig. 3 A β extracellular deposits and hp-Tau intraneuronal accumulation in the mamillary body. **a** A β deposits in the mamillary bodies, anti-A β 6F3D immunohistochemistry (scale bar 400 μ m). **b** Tau pathology (pre-tangles, tangles and threads) in the mamillary body after AT8 anti-hp-Tau immunohistochemistry (scale bar 400 μ m).

Higher magnifications of the rectangles **c** and **e** showing a peripheral stellate deposit (**c**) and a central neuritic deposit (**e**). Scale bars 20 μ m. Higher magnifications of the rectangles **d** and **f** showing axonal threads at the periphery of the mamillary body, where the PoF ends (**d**) and neurofibrillary tangles (**f**). Scale bars 20 μ m

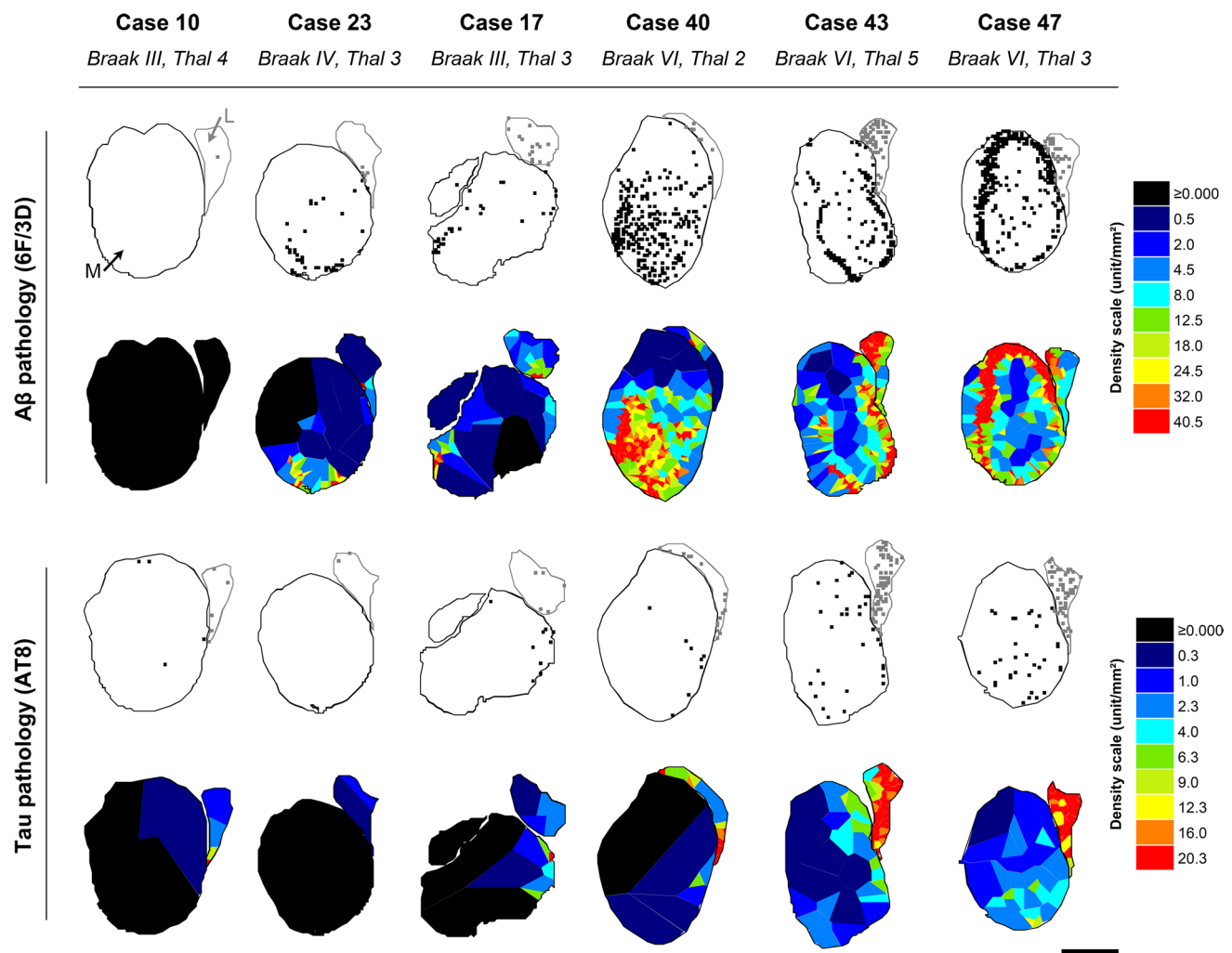


Fig. 4 Density maps of A β extracellular deposits and hp-Tau intraneuronal accumulation in the mamillary body. The maps were obtained from five post-mortem cases (listed in columns), corresponding to increased severities of A β and Tau pathologies in the mamillary body. Rows 1 and 3: maps in which the position of A β 6F3D positive extracellular deposits (row 1) or hp-Tau AT8 positive pre-NFTs, NFTs and ghost NFTs (row 3) is indicated by a dot. Black: medial nucleus (M) and grey: lateral nucleus (L) of the mamillary body. Rows 2 and 4: density maps obtained with a Voronoi (or “Dirichlet”) tessellation [16]. Polygons cover the mamillary body without interstices or overlap. Each polygon contains only one dot

(each dot corresponding to a plotted lesion) and is limited by borders located at mid-distance between the enclosed dot and its neighbours. Each point of the plane enclosed in a polygon is closer to the dot it contains than to any other dots of the map. The numerical density is inversely proportional to the polygon area (polygons are large when the lesions are wide part and small when they are close to each other) A β (row 2) or Tau (row 4) lesions. Colour scales: local density scales in unit/mm². Note that in case 40 the distribution of A β deposits was mainly central while it was peripheral and central in cases 43 and 47. The numerical density of the centrally located deposits was lower (in blue) than the density of peripherally distributed ones (red)

cytoskeleton structures or specific transport organelles in the PoF (Fig. 8b). We concluded that, as already shown by immunohistochemistry and histology, Tau accumulation in the PoF was generally made of non-fibrillary hp-Tau. Tau species found in the axons of the PoF despite the absence of fibrillary forms of the molecule or of PHF, had a seeding activity in the HEK biosensor cells.

Relationship between Tau and A β pathology

No constant hierarchical order between Tau and A β pathology

We had evidence of a propagation of hp-Tau pathology in the subiculo-fornico-mamillary system through axons. This evidence was lacking for A β . We wondered if we could find a hierarchical relationship of Tau and A β pathology among

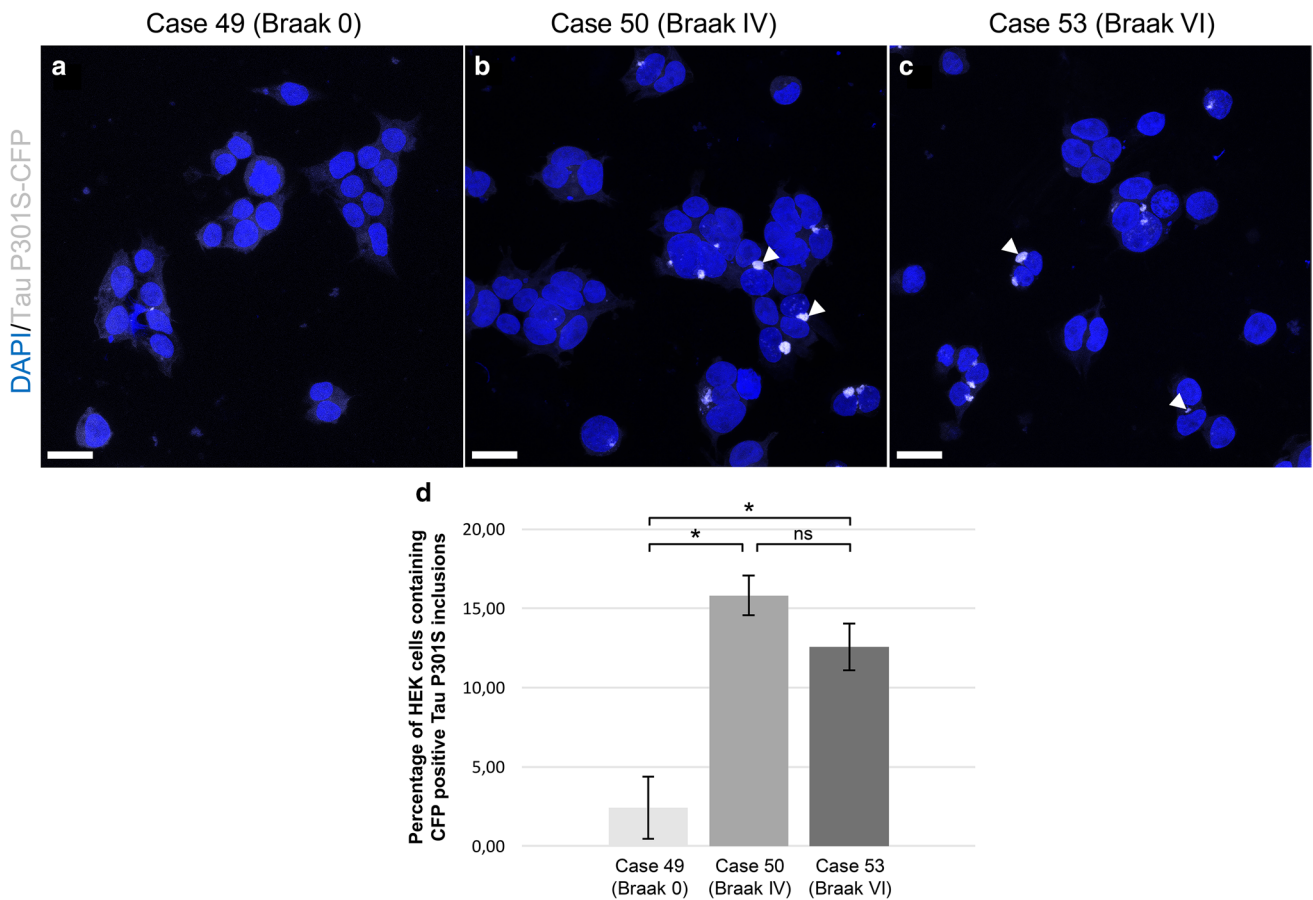


Fig. 5 Homogenates of the pillar of the fornix sampled from Alzheimer brains can act as seeds and induce Tau aggregation in vitro, in biosensor cells sensitive to Tau seeding. Homogenates of the pillar of the fornix (10% in PBS, 3000 g, 5 min) were obtained from frozen unfixed samples derived from a control case (**a**, case 49, Braak 0), a case of intermediate severity (**b**, case 50, Braak IV) and a severe Alzheimer case (**c**, case 53, Braak VI). HEK cells developed Tau P301S-CFP positive inclusions (arrowheads) when treated with homogenates from cases 50 and 53 containing Tau pathology, but not when treated

with the homogenate from the control case (case 49). Representative confocal images with maximal CFP and DAPI intensity projections from a stack of 59 sections (scale bar 20 μ m). **d** Mean percentage of HEK cells containing intracellular Tau P301S-CFP inclusions in each group, obtained after three repeated independent experiments (Student test, performed after arcsine square root transformation -applied to proportions in order to meet more closely a Gaussian distribution, *n.s.*: non-significant, $*p < 0.05$). Error bars: standard error of the mean

the cases. We could not find, however, a constant hierarchical order linking directly axonal threads or NFTs on the one hand and A β deposits on the other (Fig. 9). Yet, cross-correlation analysis of the densities of Tau and A β pathologies in the subiculo-fornico-mamillary circuit showed that the strongest correlations involved the numerical density of NFTs in the subiculum (or axonal threads in the PoF) and the volume of A β deposition in the mamillary body (supplementary Fig. 3, online resource, for detailed statistical analysis):

- NFTs in the subiculum vs. A β deposits in the mamillary body (Spearman test, $\rho_S = 0.721$, $p < 0.0001$).
- Axonal threads in the PoF vs. A β deposits in the mamillary body (Spearman test, $\rho_S = 0.718$, $p < 0.0001$).

Ten of the 16 cases without A β deposit in the mamillary body had axonal threads in the PoF, while only one of the twenty-five cases with A β deposits in the mamillary body had no axonal threads in the PoF (case 05; Fig. 9). In that case, a few threads were seen in the mamillary body, in an area encompassing the border with the hypothalamus.

Anatomical relationships

Microcryodissection could dissociate in situ axons originating from the PoF and entering the mamillary body (Fig. 10a). Some of those dissociated axonal endings were filled with Tau AT8 positive material (Fig. 10b). Microcryodissected A β focal deposits were observed in contact with

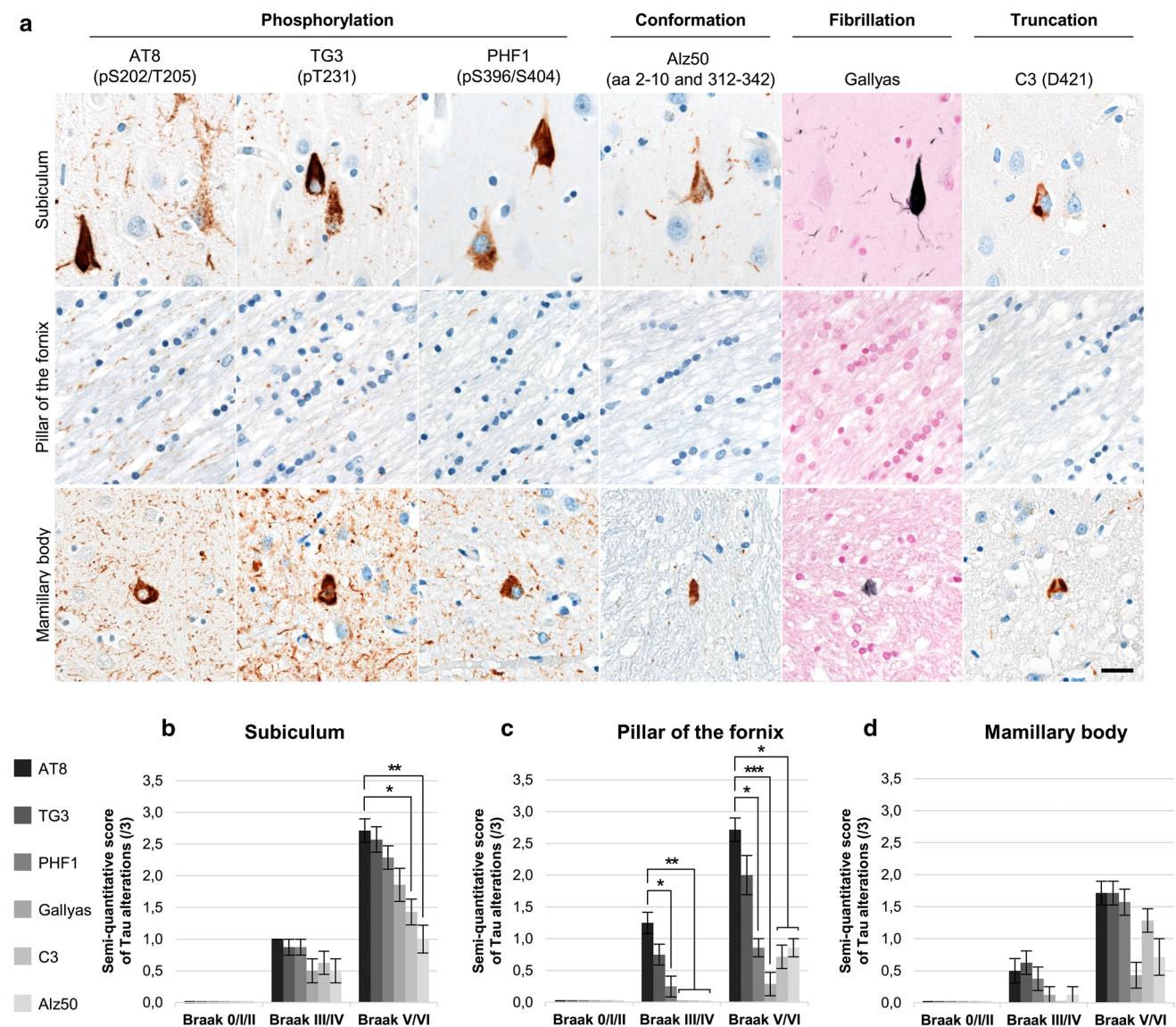


Fig. 6 Non-fibrillary hyperphosphorylated Tau is found in the axons of the pillar of the fornix. **a** Tau pathology observed in the subiculum, pillar of the fornix and mamillary body (in rows) after immunohistochemistry (IHC) against phosphorylation (AT8, TG3, PHF1), conformation (Alz50) or truncation (C3) dependent epitopes and Gallyas silver technique staining fibrillary Tau, shown in columns (scale bar: 20 μ m). Mean numerical density (semi-quantitative score) of Tau

alterations assessed in a subset of 19 cases at various Braak stages after AT8, TG3, PHF1, C3, Alz50 IHC or Gallyas silver stain in the subiculum (**b**), pillar of the fornix (**c**), mamillary body (**d**). Friedman and Dunn post-test in comparison with the values obtained after AT8 IHC, considered as the reference group (AT8): * $p < 0.05$, ** $p < 0.01$, *** $p < 0.001$. Error bars: standard error of the mean

Tau AT8 positive axonal threads in the area of the mamillary body, where fibres diverge from the bundle of the PoF (Fig. 10c).

CLARITY gave a 3D view of the various types of A β deposits observed in the mamillary body. They were either diffuse (Video 1, online resource) or cored and sometimes neuritic (Video 2, online resource). Tau positive neurites were seen entangled into A β diffuse deposits, but repelled from the amyloid core. They were sometimes in contact with A β immunoreactive material. A β deposits were observed in

the lateral and peripheral parts of the mamillary body, in the PoF terminal fields (Video 3, online resource).

Discussion

We have shown that pathological Tau found in the axons of the PoF, in the human subiculo-fornico-mamillary system, has a seeding capacity—a result that supports previous observations in cell and animal models, in which Tau

Fig. 7 Labelling profile of Tau axonal pathology in the pillar of the fornix. A subset of 19 cases at various Braak stages is listed according to the absence (–, light grey) or presence (+, dark grey) of Tau pathology in the pillar of the fornix, detected with AT8, TG3, PHF1, Alz50, C3 immunochemistry and Gallyas silver impregnation. Alz50 and C3 immunostained mainly small dots. The presence of rare dot-like immunoreactive material is indicated by “+/-”. The control group refers to Braak stages 0, I or II, the intermediate group, to Braak stages III or IV, and the severe group to Braak stages V or VI

	Cases	AT8	TG3	PHF1	Alz50	C3	Gallyas
Control	01	-	-	-	-	-	-
	04	-	-	-	-	-	-
	06	-	-	-	-	-	-
	07	-	-	-	-	-	-
Intermediate	10	+	-	-	-	-	-
	18	+	-	-	-	-	-
	14	+	+	-	-	-	-
	21	+	+	-	-	-	-
	22	+	+	-	-	-	-
	23	+	+	-	-	-	-
	19	+	+	+	-	-	-
	28	+	+	+	-	-	-
Severe	40	+	+	+	-	-	-
	43	+	+	-	+/-	+/-	-
	47	+	+	+	+	-	-
	38	+	+	+	+	+	-
	46	+	+	+	+	+	-
	44	+	+	+/-	+/-	+/-	+
	45	+	+	+	+	+/-	+

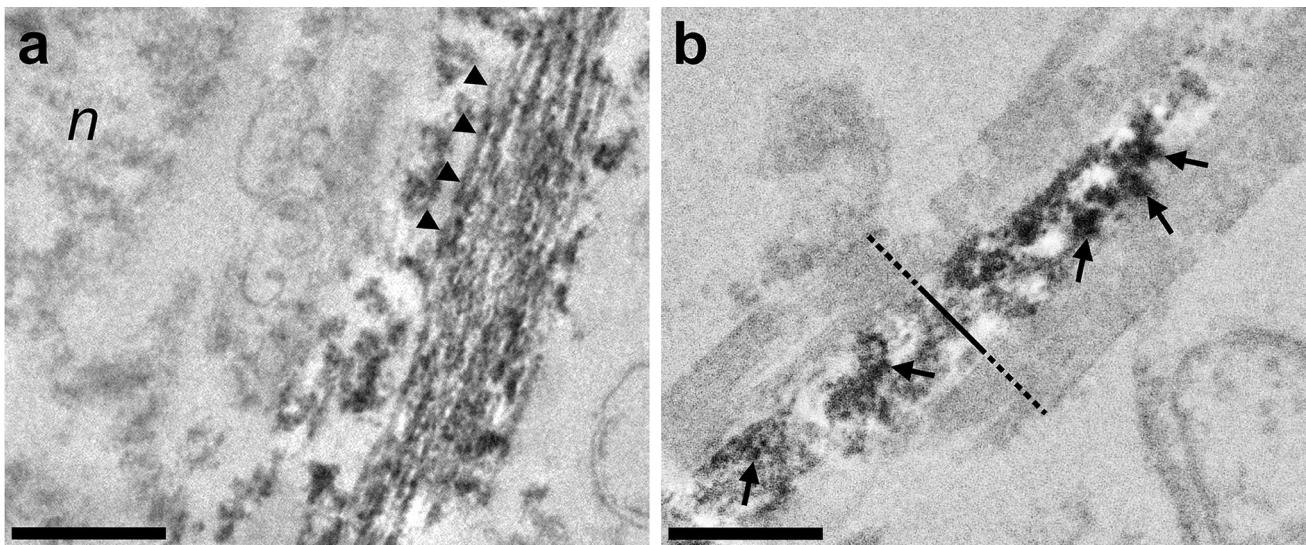


Fig. 8 Intra-axonal aggregates of hyperphosphorylated Tau, devoid of PHF, in the pillar of the fornix. Diaminobenzidine electron-dense precipitates observed at electron microscopy after AT8 anti-hp-Tau immunohistochemistry in the subiculum (a) or in the pillar of the fornix (b) of an Alzheimer case (Braak VI, Thal 5; scale bar 500 nm). a AT8 labelled PHFs located in the perikaryon of a neuron in the

subiculum (arrowheads). n nucleus. b hp-Tau AT8 positive staining (arrows) in an axon of the pillar of the fornix, devoid of any PHF. AT8 immunoreactivity was located in the axoplasm (solid line) and absent in the myelin sheath (dashed line). We could not identify cytoskeleton components or organelles associated with hp-Tau immunoreactivity

pathology is transmitted from cell to cell through neuronal connections [8, 10, 32, 40, 57, 58, 65]. The study of Tau pathology in the subiculum, in the PoF, one of its major efferent tracts and in the mamillary body, its main projection area, suggested that Tau pathology progressed in an anterograde direction. Tau aggregates in the cell body of the subicular neurons were immunolabelled by antibodies against hp-Tau (AT8, TG3 and PHF1), misfolded Tau

(Alz50) and N-truncated Tau (C3) and silver stained with Gallyas method, which is thought to stain only fibrillary Tau structures. The PHF nature of the aggregates was confirmed by electron microscopy. The PoF was cut longitudinally to facilitate the analysis of the fibre tract. The axons of the PoF, principally issued from the subicular neurons, were, by contrast, preferentially immunolabelled by AT8 and TG3 antibodies, less extensively by PHF1 antibody,

Fig. 9 No relationship could be observed between Tau and A β pathology distribution. Cases listed according to the absence (–, light grey) or presence (+, dark grey) of Tau or A β pathology in the subiculum (sub-Tau or sub-A β), pillar of the fornix (PoF–Tau or PoF–A β) and mamillary body (MB–Tau or MB–A β). NB: Six mamillary bodies could not be sampled; the six corresponding cases were excluded from the analysis of the hierarchical distribution (in grey, end of the table)

Cases	Sub-Tau	Sub-A β	PoF-Tau	PoF-A β	MB-Tau	MB-A β
01	-	-	-	-	-	-
02	-	-	-	-	-	-
04	-	-	-	-	-	-
06	-	-	-	-	-	-
07	-	-	-	-	-	-
05	-	+	-	-	-	+
24	+	-	-	-	-	-
11	+	-	+	-	-	-
13	+	-	+	-	-	-
16	+	-	+	-	-	-
19	+	-	+	-	-	-
20	+	-	+	-	-	-
21	+	-	+	-	-	-
14	+	+	+	-	-	-
09	+	+	+	-	-	+
23	+	+	+	-	-	+
29	+	+	+	-	-	+
37	+	+	+	-	-	+
18	+	-	+	-	+	-
28	+	-	+	-	+	-
10	+	+	+	-	+	-
17	+	+	+	-	+	+
22	+	+	+	-	+	+
25	+	+	+	-	+	+
26	+	+	+	-	+	+
30	+	+	+	-	+	+
31	+	+	+	-	+	+
32	+	+	+	-	+	+
33	+	+	+	-	+	+
34	+	+	+	-	+	+
36	+	+	+	-	+	+
38	+	+	+	-	+	+
39	+	+	+	-	+	+
40	+	+	+	-	+	+
41	+	+	+	-	+	+
42	+	+	+	-	+	+
43	+	+	+	-	+	+
44	+	+	+	-	+	+
45	+	+	+	-	+	+
46	+	+	+	-	+	+
47	+	+	+	-	+	+
03	-	-	-	-	/	/
08	-	-	-	-	/	/
15	+	-	+	-	/	/
12	+	+	+	-	/	/
27	+	+	+	-	/	/
35	+	+	+	-	/	/

and were devoid of any PHF except in two severe cases. We were able to show that these non-fibrillary molecular species had a seeding activity on the Tau P301S HEK biosensor cells. The seeding activity was independent from N-truncated Tau (no C3 positive threads), aggregated Tau (no Gallyas positive threads) or PHF (no PHF at electron microscopy) and was associated with a high concentration of Tau phosphorylated at the specific sites Ser202/

Thr205 and Thr231, recognised by AT8 and TG3 antibodies. This suggested that the axons of the PoF, containing but a subset of the Tau species detected in the cell body of the subicular neurons, could transmit pathology to the neurons of the mamillary body that secondarily acquired the same, and complete, immunolabelling and staining profile as those of the subiculum. We could not find any

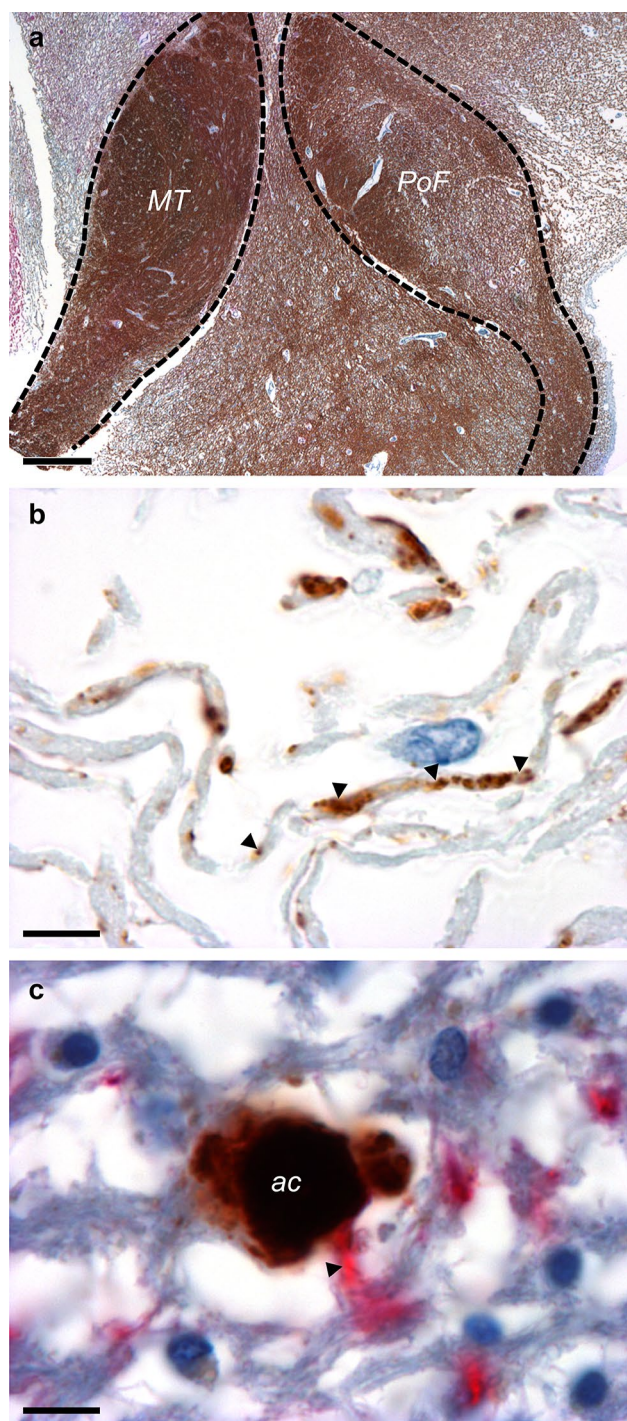


Fig. 10 Hyperphosphorylated-Tau positive axonal threads are in contact with A β deposits in the mamillary body. **a** Coronal section of the mamillary body after microcryodissection. Preserved aspect of the microcryodissected section at low magnification. Anti-MBP/NF immunohistochemistry (myelin basic protein—MBP—in brown, neurofilament—NF—in red). PoF: end of the afferent pillar of the fornix. MT: origin of the efferent mamillo-thalamic tract (scale bar 400 μ m). **b** Isolated axons of the pillar of the fornix filled with hp-Tau AT8 positive material (arrowheads), observed in the mamillary body after microcryodissection. Anti-hp-Tau AT8 immunohistochemistry (scale bar 8 μ m). **c** Microcryodissected A β focal deposit in contact with a hp-Tau AT8 positive axonal thread (arrowhead) in the mamillary body. Anti-A β 6F3D/hp-Tau AT8 immunohistochemistry (A β in brown, Tau in red, scale bar 8 μ m). *ac* amyloid core

influence of α -synuclein pathology on Tau aggregation and A β deposition in the subiculo-fornico-mamillary system.

The NFT seen in the subiculum preceded the appearance of threads in the PoF. The presence of AT8 positive threads in the PoF has already been described [49]. The authors also mentioned AT8 positive astrocytes in the mamillary body. We considered, as they did, that these were changes characteristic of aging-related tau astrogliopathy (ARTAG). We completed the study of Plowey and Ziskin [49] by studying the PoF tangentially to its direction: this procedure allowed us to have a better view on the Tau positive threads. As mentioned, we also characterised the immunological profile of the threads and showed that they had a seeding activity despite the absence of PHF demonstrated by electron microscopy.

Tau hyperphosphorylation has been shown to strongly contribute to the seeding efficiency and propagation capacity of Tau [39]. Recent evidence, however, indicates that the conformation of Tau protein, independently of its phosphorylation state, is crucial [48]. The abnormal conformations of Tau in the PHF of AD [23, 25] and of chronic traumatic encephalopathy [24] and in Pick's bodies [22] have been described at the molecular level with cryo-EM, but PHF could be a final change that occurs late, while the seeding properties may be present early in the course of Tau alteration. It has been shown that misfolded monomers actually play an essential role in the seeding of Tau pathology [48, 55], but their conformation has not been elucidated. It could be similar or different from the conformation described in PHF. The sequence (VQIINK/VQIVYK) that is exposed in the seeding monomers and is thought to be important for their aggregation [48, 64], could be engaged in the fibrillation, after the initial seeding.

In all the cases with accumulation of A β in the mamillary body, A β had also accumulated in the subiculum, while two cases with A β accumulation in the subiculum had none in the mamillary body. This regional distribution is compatible with a transmission of A β pathology from the subiculum to the mamillary body (as already suggested by Thal et al. [59], see their Fig. 6). However, we could not find any histological or biochemical evidence of a transport of A β through the PoF. This negative result does not preclude the possibility of a transfer of soluble species such as oligomers. As far as we know, there is currently no biosensor yet available to detect A β aggregation seeding activity. It has been repeatedly emphasised that the progression of A β pathology through the brain was not only related to connections, but to other possible pathways such as diffusion through extracellular space or through basal membrane [20]: in the human, Tau pathology was absent from—and A β accumulated in—a disconnected piece of cortex in a patient with AD [17]; transmission of A β pathology may occur through contaminated dural graft

[37, 43], injection of contaminated cadaver-derived growth hormone or, possibly, neurosurgical procedures [9, 19, 41, 42, 51]. In transgenic mice, A β deposits may develop in the brain after intraperitoneal injection of A β -containing brain extracts [21]. Because the mamillary body is not contiguous with the subiculum, passive diffusion through the subiculo-mamillary system is less probable than axonal transport through the PoF.

We attempted to find a link between Tau aggregation and A β accumulation in the subiculo-fornico-mamillary system. Although there was indeed a strong correlation between the volume densities of A β deposits and the semi-quantitative score of Tau in the subiculum, fornix and mamillary body, we were unable to demonstrate a hierarchical order that would suggest a cause-and-effect relationship: in three cases, the presence of Tau NFTs in the mamillary body was not associated with A β deposits; in five cases in which A β deposits were seen, there was no Tau aggregates in the mamillary body. A cause-and-effect relationship between A β accumulation and Tau aggregates has been sought for decades [4, 45]: in the cascade hypothesis, A β accumulation causes Tau aggregates [33]. It should, however, be emphasised that Tau aggregation has never been observed in APP or APP \times PS1 transgenic mice even in animals expressing human Tau. In the opposite scenario, only tangle-bearing neurons are able to produce fibrillary A β [4], but aggregation of abnormal Tau, sharing the immunohistochemical properties of AD Tau, is not always associated with A β accumulation [3], see figure in [15]. A third scenario remains to be discussed: the relationship between A β deposition and Tau aggregation could be a promotion of the second by the first, rather than a link of cause-and-effect. A β deposition, indeed, promotes Tau aggregation and diffusion [35, 52, 63], possibly through an interaction with the prion protein [28], but, by contrast, Tau aggregation does not promote A β deposition [36, 44, 50]. In the subiculo-fornico-mamillary system, the distribution of the lesions strongly suggests that pathology is initiated by Tau aggregation in the subiculum. Tau aggregation appears to follow the anterograde direction, affecting first the PoF and reaching secondarily the mamillary body. It is correlated with A β accumulation, but this correlation is not a consequence of a cause-and-effect relationship: there is at least one case of A β accumulation that is not associated with Tau pathology and there are several cases of Tau aggregation without A β accumulation. In agreement with this absence of causality, experimental evidence suggests that the correlation is rather due to a promotion of Tau aggregation by A β : when A β accumulation, independently initiated, keeps progressing, it tends to promote Tau pathology. The simultaneous increase of Tau and A β pathology explains the positive correlation. The interaction between Tau aggregation and A β accumulation probably takes place in the senile

plaque: microcryodissection and CLARITY indeed show a physical interaction of both pathologies at that level.

Acknowledgements This project received financial support from France Alzheimer (project “Propagation of Tau and A β aggregation through axons in the subiculo-fornico-mamillary system: tracking propagons” and Ibis (Project “Neuro-CEB better”). Manon Thierry was funded by a doctoral scholarship from the Ministry of Research and Higher Education, attributed by the doctoral school “Physiology, Physiopathology and Therapeutics-ED394” (Sorbonne University). The human samples were obtained from the Neuro-CEB brain bank (BRIF Number 0033-00011), partly funded by the patients’ associations ARSEP, ARSLA, “Connaître les Syndromes Cérébelleux”, France-DFT, France Parkinson and by Vaincre Alzheimer Fondation, to which we express our gratitude. We are also grateful to the patients and their families. We thank Sabrina Leclère-Turbant and Marie-Claire Artaud for their technical and managerial assistance with post-mortem human samples. The brain bank is hosted by the Biological Resources Platform of Pitié-Salpêtrière Hospital, APHP. Brain clarification with CLARITY was performed on the ICM HISTOMICS platform. Cell culture experiments were performed on the ICM CELIS platform. Biphoton, confocal and electronic microscopy pictures were acquired on the ICM. QUANT imaging platform. We thank the technical team of the Raymond Escourrolle neuropathology department as well as the technical staff involved at ICM, including Valérie Thuries and Annick Prigent for their help and technical advices in histology, Julien Dumont for his assistance and expertise in CLARITY-cleared tissue imaging and analysis and Dominique Langui and Asha Baskaran for their help and knowledge in electron microscopy analysis. We also thank Jean-Pierre Brion and Kunie Ando for their valuable advices and discussion. The Neuro-CEB Neuropathology network includes: Dr. Franck Letournel (CHU Angers), Dr. Marie-Laure Martin-Négrier (CHU Bordeaux), Pr. Françoise Chapon (CHU Caen), Pr. Catherine Godfraind (CHU Clermont-Ferrand), Pr. Claude-Alain Maurage (CHU Lille), Dr. Vincent Deramecourt (CHU Lille), Dr. David Meyronnet (CHU Lyon), Dr. Nathalie Streichenberger (CHU Lyon), Dr. André Maues de Paula (CHU Marseille), Pr. Valérie Rigau (CHU Montpellier), Dr. Fanny Vandenbos-Burel (Nice), Pr. Charles Duyckaerts (CHU PS Paris), Pr. Danielle Seilhean (CHU PS, Paris), Dr. Susana Boluda (CHU PS, Paris), Dr. Isabelle Plu (CHU PS, Paris), Dr. Serge Milin (CHU Poitiers), Dr. Dan Christian Chiforeanu (CHU Rennes), Pr. Annie Laquerrière (CHU Rouen), Dr. Béatrice Lannes (CHU Strasbourg).

References

1. Ando K, Laborde Q, Lazar A, Godefroy D, Youssef I, Amar M et al (2014) Inside Alzheimer brain with CLARITY: senile plaques, neurofibrillary tangles and axons in 3-D. *Acta Neuropathol* 128:457–459. <https://doi.org/10.1007/s00401-014-1322-y>
2. Braak H, Braak E (1991) Neuropathological staging of Alzheimer-related changes. *Acta Neuropathol* 82:239–259
3. Braak H, Braak E (1997) Frequency of stages of Alzheimer-related lesions in different age categories. *Neurobiol Aging* 18:351–357
4. Braak H, Del Tredici K (2013) Amyloid- β may be released from non-junctional varicosities of axons generated from abnormal tau-containing brainstem nuclei in sporadic Alzheimer’s disease: a hypothesis. *Acta Neuropathol* 126:303–306. <https://doi.org/10.1007/s00401-013-1153-2>
5. Braak H, Braak E, Grundke-Iqbal I, Iqbal K (1986) Occurrence of neuropil threads in the senile human brain and in Alzheimer’s disease: a third location of paired helical filaments outside of neurofibrillary tangles and neuritic plaques. *Neurosci Lett* 65:351–355

6. Braak H, Del Tredici K, Rüb U, De Vos RAI, Jansen Steur ENH, Braak E (2003) Staging of brain pathology related to sporadic Parkinson's disease. *Neurobiol Aging* 24:197–211. [https://doi.org/10.1016/S0197-4580\(02\)00065-9](https://doi.org/10.1016/S0197-4580(02)00065-9)
7. Brion JP, Passareiro H, Nunez J, Flament-Durand J (1985) Mise en évidence immunologique de la protéine Tau au niveau des lésions de dégénérescence neurofibrillaire de la maladie d'Alzheimer. *Arch Biol (Bruxelles)* 95:229–235
8. Calafate S, Buist A, Miskiewicz K, Vijayan V, Daneels G, de Strooper B et al (2015) Synaptic contacts enhance cell-to-cell tau pathology propagation. *Cell Rep* 11:1176–1183. <https://doi.org/10.1016/j.celrep.2015.04.043>
9. Cali I, Cohen ML, Haik S, Parchi P, Giaccone G, Collins SJ et al (2018) Iatrogenic Creutzfeldt–Jakob disease with Amyloid- β pathology: an international study. *Acta Neuropathol Commun* 6:5. <https://doi.org/10.1186/s40478-017-0503-z>
10. Clavaguera F, Bolmont T, Crowther RA, Abramowski D, Frank S, Probst A et al (2009) Transmission and spreading of tauopathy in transgenic mouse brain. *Nat Cell Biol* 11:909–913. <https://doi.org/10.1038/ncb1901>
11. Copenhagen BR, Rabin LA, Saykin AJ, Roth RM, Wishart HA, Flashman LA et al (2006) The fornix and mammillary bodies in older adults with Alzheimer's disease, mild cognitive impairment, and cognitive complaints: a volumetric MRI study. *Psychiatry Res Neuroimaging* 147:93–103. <https://doi.org/10.1016/j.psychres.2006.01.015>
12. Crary JF, Trojanowski JQ, Schneider JA, Abisambra JF, Abner EL, Alafuzoff I et al (2014) Primary age-related tauopathy (PART): a common pathology associated with human aging. *Acta Neuropathol* 128:755–766. <https://doi.org/10.1007/s00401-014-1349-0>
13. Delaère P, Duyckaerts C, He Y, Piette F, Hauw JJ (1991) Subtypes and differential laminar distributions of beta A4 deposits in Alzheimer's disease: relationship with the intellectual status of 26 cases. *Acta Neuropathol* 81:328–335. <https://doi.org/10.1007/bf00305876>
14. Duyckaerts C, Godefroy G (2000) Voronoi tessellation to study the numerical density and the spatial distribution of neurones. *J Chem Neuroanat* 20:83–92. [https://doi.org/10.1016/s0891-0618\(00\)00064-8](https://doi.org/10.1016/s0891-0618(00)00064-8)
15. Duyckaerts C, Hauw J-J (1997) Prevalence, incidence and duration of Braak's stages in the general population: can we know? *Neurobiol Aging* 18:362–369
16. Duyckaerts C, Godefroy G, Hauw JJ (1994) Evaluation of neuronal numerical density by Dirichlet tessellation. *J Neurosci Methods* 51:47–69. [https://doi.org/10.1016/0165-0270\(94\)90025-6](https://doi.org/10.1016/0165-0270(94)90025-6)
17. Duyckaerts C, Uchihara T, Seilhean D, He Y, Hauw J-J (1997) Dissociation of Alzheimer type pathology in a disconnected piece of cortex. *Acta Neuropathol* 93:501–507
18. Duyckaerts C, Braak H, Brion J-P, Buée L, Del Tredici K, Goedert M et al (2015) PART is part of Alzheimer disease. *Acta Neuropathol* 129:749–756. <https://doi.org/10.1007/s00401-015-1390-7>
19. Duyckaerts C, Sazdovitch V, Ando K, Seilhean D, Privat N, Yilmaz Z et al (2018) Neuropathology of iatrogenic Creutzfeldt–Jakob disease and immunoassay of French cadaver-sourced growth hormone batches suggest possible transmission of tauopathy and long incubation periods for the transmission of A β pathology. *Acta Neuropathol* 135:201–212. <https://doi.org/10.1007/s00401-017-1791-x>
20. Eisele YS, Duyckaerts C (2016) Propagation of A β pathology: hypotheses, discoveries, and yet unresolved questions from experimental and human brain studies. *Acta Neuropathol* 131:5–25
21. Eisele YS, Obermuller U, Heilbronner G, Baumann F, Kaeser SA, Wolburg H et al (2010) Peripherally applied A β -containing inoculates induce cerebral β -amyloidosis. *Science* 330:980–982. <https://doi.org/10.1126/science.1194516>
22. Falcon B, Zhang W, Murzin AG, Murshudov G, Garringer HJ, Vidal R et al (2018) Structures of filaments from Pick's disease reveal a novel tau protein fold. *Nature* 561:137–140. <https://doi.org/10.1038/s41586-018-0454-y>
23. Falcon B, Zhang W, Schweighauser M, Murzin AG, Vidal R, Garringer HJ et al (2018) Tau filaments from multiple cases of sporadic and inherited Alzheimer's disease adopt a common fold. *Acta Neuropathol* 136:699–708. <https://doi.org/10.1007/s00401-018-1914-z>
24. Falcon B, Zivanov J, Zhang W, Murzin AG, Garringer HJ, Vidal R et al (2019) Novel tau filament fold in chronic traumatic encephalopathy encloses hydrophobic molecules. *Nature* 568:420–423. <https://doi.org/10.1038/s41586-019-1026-5>
25. Fitzpatrick AWP, Falcon B, He S, Murzin AG, Murshudov G, Garringer HJ et al (2017) Cryo-EM structures of tau filaments from Alzheimer's disease. *Nature* 547:185–190. <https://doi.org/10.1038/nature23002>
26. Furman JL, Holmes BB, Diamond MI (2015) Sensitive detection of proteopathic seeding activity with FRET flow cytometry. *J Vis Exp*. <https://doi.org/10.3791/53205>
27. Gallyas F (1971) Silver staining of Alzheimer's neurofibrillary changes by means of physical development. *Acta Morphol Acad Sci Hung* 19:1–8
28. Gomes LA, Hipp SA, Rijal Upadhaya A, Balakrishnan K, Ospitalieri S, Koper MJ et al (2019) A β -induced acceleration of Alzheimer-related τ -pathology spreading and its association with prion protein. *Acta Neuropathol* 138:913–941. <https://doi.org/10.1007/s00401-019-02053-5>
29. Grignon Y, Duyckaerts C, Bennece M, Hauw J-J (1998) Cytoarchitectonic alterations in the supramarginal gyrus of late onset Alzheimer's disease. *Acta Neuropathol* 95:395–406
30. Grundke-Iqbal I, Iqbal K, Tung YC, Quinlan M, Wisniewski HM, Binder LI (1986) Abnormal phosphorylation of the microtubule-associated protein tau (τ) in Alzheimer cytoskeletal pathology. *Proc Natl Acad Sci* 83:4913–4917. <https://doi.org/10.1073/pnas.83.13.4913>
31. Gundersen HJ, Osterby R (1981) Optimizing sampling efficiency of stereological studies in biology: or “do more less well!”. *J Microsc* 121:65–73
32. Guo JL, Narasimhan S, Changolkar L, He Z, Stieber A, Zhang B et al (2016) Unique pathological tau conformers from Alzheimer's brains transmit tau pathology in nontransgenic mice. *J Exp Med* 213:2635–2654. <https://doi.org/10.1084/jem.20160833>
33. Hardy JA, Higgins GA (1992) Alzheimer's disease: the amyloid cascade hypothesis. *Science* 256:184–185
34. Hauw J, Feske S, Amarenco P, De Girolami U (2019) Vascular pathology. In: Gray F, Duyckaerts C, De Girolami U (eds) *Manual of basic neuropathology*, 6th edn. Oxford University Press, Oxford, pp 82–121
35. He Z, Guo JL, McBride JD, Narasimhan S, Kim H, Changolkar L et al (2017) Amyloid- β plaques enhance Alzheimer's brain tau-seeded pathologies by facilitating neuritic plaque tau aggregation. *Nat Med* 24:29–38. <https://doi.org/10.1038/nm.4443>
36. Héraud C, Goufak D, Ando K, Leroy K, Suain V, Yilmaz Z et al (2014) Increased misfolding and truncation of tau in APP/PS1/tau transgenic mice compared to mutant tau mice. *Neurobiol Dis* 62:100–112. <https://doi.org/10.1016/j.nbd.2013.09.010>
37. Hervé D, Porché M, Cabrejo L, Guidoux C, Tournier-Lasserre E, Nicolas G et al (2018) Fatal A β cerebral amyloid angiopathy 4 decades after a dural graft at the age of 2 years. *Acta Neuropathol* 135:801–803. <https://doi.org/10.1007/s00401-018-1828-9>
38. Holmes BB, Furman JL, Mahan TE, Yamasaki TR, Mirbaha H, Eades WC et al (2014) Proteopathic tau seeding predicts tauopathy in vivo. *Proc Natl Acad Sci USA* 111(41):E4376–E4385. <https://doi.org/10.1073/pnas.1411649111>

39. Hu W, Zhang X, Tung YC, Xie S, Liu F, Iqbal K (2016) Hyperphosphorylation determines both the spread and the morphology of tau pathology. *Alzheimer's Dement* 12:1066–1077. <https://doi.org/10.1016/j.jalz.2016.01.014>
40. Iba M, McBride JD, Guo JL, Zhang B, Trojanowski JQ, Lee VM-Y (2015) Tau pathology spread in PS19 tau transgenic mice following locus coeruleus (LC) injections of synthetic tau fibrils is determined by the LC's afferent and efferent connections. *Acta Neuropathol* 130:349–362. <https://doi.org/10.1007/s00401-015-1458-4>
41. Jaunmuktane Z, Mead S, Ellis M, Wadsworth JDF, Nicoll AJ, Kenny J et al (2015) Evidence for human transmission of amyloid- β pathology and cerebral amyloid angiopathy. *Nature* 525:247–250. <https://doi.org/10.1038/nature15369>
42. Jaunmuktane Z, Quaegebeur A, Taipa R, Viana-Baptista M, Barbosa R, Koriath C et al (2018) Evidence of amyloid- β cerebral amyloid angiopathy transmission through neurosurgery. *Acta Neuropathol* 135:671–679. <https://doi.org/10.1007/s00401-018-1822-2>
43. Kovacs GG, Lutz MI, Ricken G, Ströbel T, Höftberger R, Preusser M et al (2016) Dura mater is a potential source of A β seeds. *Acta Neuropathol* 131:911–923. <https://doi.org/10.1007/s00401-016-1565-x>
44. Lewis J, Dickson DW, Lin W, Chisholm L, Corral A, Jones G et al (2001) Enhanced neurofibrillary degeneration in transgenic mice expressing mutant Tau and APP. *Science* 293:1487–1491
45. Mann DMA, Hardy J (2013) Amyloid or tau: the chicken or the egg? *Acta Neuropathol* 126:609–613. <https://doi.org/10.1007/s00401-013-1162-1>
46. McKeith IG, Boeve BF, Dickson DW, Halliday G, Taylor J-P, Weintraub D et al (2017) Diagnosis and management of dementia with Lewy bodies. *Neurology* 89:88–100. <https://doi.org/10.1212/WNL.0000000000004058>
47. Meyer-Luehmann M, Coomaraswamy J, Bolmont T, Kaeser S, Schaefer C, Kilger E et al (2006) Exogenous induction of cerebral β -amyloidogenesis is governed by agent and host. *Science* 313:1781–1784. <https://doi.org/10.1126/science.1131864>
48. Mirbaha H, Chen D, Morazova OA, Ruff KM, Sharma AM, Liu X et al (2018) Inert and seed-competent tau monomers suggest structural origins of aggregation. *Elife* 7:e36584. <https://doi.org/10.7554/eLife.36584>
49. Plowey ED, Ziskin JL (2016) Hippocampal phospho-tau/MAPT neuropathology in the fornix in Alzheimer disease: an immunohistochemical autopsy study. *Acta Neuropathol Commun* 4:114. <https://doi.org/10.1186/s40478-016-0388-2>
50. Pooler AM, Polydoro M, Maury EA, Nicholls SB, Reddy SM, Wegmann S et al (2015) Amyloid accelerates tau propagation and toxicity in a model of early Alzheimer's disease. *Acta Neuropathol Commun* 3:14. <https://doi.org/10.1186/s40478-015-0199-x>
51. Ritchie DL, Adlard P, Peden AH, Lowrie S, Le Grice M, Burns K et al (2017) Amyloid- β accumulation in the CNS in human growth hormone recipients in the UK. *Acta Neuropathol* 134:221–240. <https://doi.org/10.1007/s00401-017-1703-0>
52. Saito T, Mihira N, Matsuba Y, Sasaguri H, Hashimoto S, Narasimhan S et al (2019) Humanization of the entire murine Mapt gene provides a murine model of pathological human tau propagation. *J Biol Chem* 294:12754–12765. <https://doi.org/10.1074/jbc.RA119.009487>
53. Schmidt ML, Lee VM, Trojanowski JQ (1991) Comparative epitope analysis of neuronal cytoskeletal proteins in Alzheimer's disease senile plaque neurites and neuropil threads. *Lab Invest* 64:352–357
54. Selkoe DJ, Hardy J (2016) The amyloid hypothesis of Alzheimer's disease at 25 years. *EMBO Mol Med* 8:595–608. <https://doi.org/10.15252/emmm.201606210>
55. Sharma AM, Thomas TL, Woodard DR, Kashmer OM, Diamond MI (2018) Tau monomer encodes strains. *Elife*. <https://doi.org/10.7554/eLife.37813>
56. Snedecor G, Cochran W (1980) *Statistical methods*, 7th edn. Iowa State University Press, Ames, pp 290–291
57. Takeda S, Wegmann S, Cho H, DeVos SL, Commins C, Roe AD et al (2015) Neuronal uptake and propagation of a rare phosphorylated high-molecular-weight tau derived from Alzheimer's disease brain. *Nat Commun* 6:8490. <https://doi.org/10.1038/ncomms9490>
58. Tardivel M, Bégard S, Bousset L, Dujardin S, Coens A, Melki R et al (2016) Tunneling nanotube (TNT)-mediated neuron-to-neuron transfer of pathological Tau protein assemblies. *Acta Neuropathol Commun* 4:117. <https://doi.org/10.1186/s40478-016-0386-4>
59. Thal DR, Rüb U, Orantes M, Braak H (2002) Phases of A β -deposition in the human brain and its relevance for the development of AD. *Neurology* 58:1791–1800
60. Thierry M, Marty S, Boluda S, Duyckaerts C (2017) Alzheimer's senile plaque as shown by microcryodissection, a new technique for dissociating tissue structures. *J Neural Transm* 124:685–694. <https://doi.org/10.1007/s00702-017-1718-7>
61. Uchihara T, Kondo H, Ikeda K, Kosaka K (1995) Alzheimer-type pathology in melanin-bleached sections of substantia nigra. *J Neurol* 242:485–489
62. Vann SD, Aggleton JP (2004) The mammillary bodies: two memory systems in one? *Nat Rev Neurosci* 5:35–44. <https://doi.org/10.1038/nrn1299>
63. Vergara C, Houben S, Suain V, Yilmaz Z, De Decker R, Vanden Dries V et al (2019) Amyloid- β pathology enhances pathological fibrillary tau seeding induced by Alzheimer PHF in vivo. *Acta Neuropathol* 137:397–412. <https://doi.org/10.1007/s00401-018-1953-5>
64. von Bergen M, Friedhoff P, Biernat J, Heberle J, Mandelkow E-M, Mandelkow E (2000) Assembly of tau protein into Alzheimer paired helical filaments depends on a local sequence motif (306VQIVYK311) forming beta structure. *Proc Natl Acad Sci* 97:5129–5134. <https://doi.org/10.1073/pnas.97.10.5129>
65. Wang Y, Balaji V, Kaniyappan S, Krüger L, Irsen S, Tepper K et al (2017) The release and trans-synaptic transmission of Tau via exosomes. *Mol Neurodegener* 12:5. <https://doi.org/10.1186/s13024-016-0143-y>
66. Weibel ER (1979) *Stereological methods, vol. 1: practical methods for biological morphometry*. Academic, London

Publisher's Note Springer Nature remains neutral with regard to jurisdictional claims in published maps and institutional affiliations.